FINAL TECHNICAL REPORT
(December 31, 2007)

Project Title: Seismic illumination of temporal-spatial patterns of damage on the San Andreas fault, Parkfield in 4D

Award Number: 07HQGR0033

Sponsor: US Geological Survey

Principal Investigator: Yong-Gang Li
Department of Earth Sciences
University of Southern California
Los Angeles, CA 90089-0740
E-mail: ygli@terra.usc.edu
Tel: 213-740-3556
Fax: 213-740-8801

Proposed Start Date: January 1, 2007

Proposed Duration: 12 months.

Key Words: Fault-Zone Trapped Wave, Fault Damage and Healing, Dynamic Rupture

Non-technical Summary:

Highly damaged fault rocks along the San Andreas Fault at Parkfield create a low velocity zone that can trap seismic waves from both earthquakes and explosions [*Li et al.*, 2004]. We have modeled these types of fault-zone trapped waves (FZTWs) waves using finite difference methods. The models suggest that, on average, a fault zone cross section consist of a composite of two sub-vertical layers, one a 30 m-wide fault core, the other a surrounding 100-200 m wide damage zone. The damage zone velocities range between 65-75% of the fault zone wall rocks, while those of the core are even less, going as low as 50% of the intact rock [*Li et al.*, 2004]. Down-hole seismographs emplaced in the SAFOD Main Hole at ~3 km depths also register prominent Fg waves from deeper events. The width and velocity reduction of the damage zone at this depth as delineated by fault-zone trapped waves has been verified by the SAFOD drilling and logging studies. These studies show that a ~200 m-wide zone of high porosity, multiple slip planes, and average velocity reductions of ~30-35% is present at these depths. Thus this is the minimum depth to which the low velocity layers extend. Observations and models of FZTWs generated by microearthquakes at different focal depths suggest that this type of fault structure reaches to depths of ~7 km or more. In fact, while the velocity contrasts and layer thickness appear to become smaller with increasing depth, it is likely that a low velocity fault guided "channel" extend across the entire seismogenic depth at Parkfield. The damage zone of the SAF is not laterally symmetric. Instead, it appears to extend farther into the SW side of the fault. This could be due to rocks already weakened from previous faulting. It could also be due to greater damage in the extensional quadrant near the propagating crack tip of Parkfield earthquakes. We interpret the low-velocity waveguide as being a zone of accumulated damage from recurrent major earthquakes, including the 2004 *M*6 earthquake. This type of damage varies with depth and also along the strike, and may relate to the on- and near-fault variations in stress and slip distribution during earthquake rupture.

Intellectual Merit and Broader Impact. So far, because of the density and frequency of our data, this study may be the first to illuminate the temporal-spatio patterns of damage on a major fault zone due a *M*6 earthquake in 4-D. In contrast to the Landers and Hector Mine earthquakes examined previously, in the present case, our deployments straddle the mainshock and thus we are able to isolate co-seismic changes as well as the post-mainshock healing. The results have implications for the physics of co-seismic and post-seismic faulting processes. Further, because of the types and quality of our observations, our work provides fundamental information on the nature and source of the fault damage in situ. This research will help to develop and test models of large and small earthquake occurrence at Parkfield.

The work done through this project helps to determine the evolution of physical properties that might control the onset and characteristics of damaging earthquakes. As part of this exercise, the *M*6 Parkfield earthquake can be taken as a validation test to assess the faulting process on active faults globally. This study is to utilize data collected by USC, Duke University, USGS and SAFOD of EarthScope at Parkfield. The project involves graduate student and Post-doctorial research and scholarly exchange between USC and other institutions.

ACTIVITIES:

We have systematically examined the data recorded in several active and passive seismic experiments near the SAFOD site before and after the 2004 *M*6 Parkfield earthquake [*Li et al.*, 2006, 2007]. These experiments indicate that the Parkfield low-velocity zone weakened co-seismically, and then healed back toward its pre-earthquake state over a period of several months to several years. Waveform cross-correlation measurements from repeated explosions and microearthquakes suggest that a peak decrease of ~2.5% in velocity occurred coseismically within the fault zone at seismogenic depths. Measurements from repeating aftershocks show that a ~1.2% velocity increase occurred within the fault zone in the first 3-4 months after the mainshock. The healing rate appears to be approximately logarithmic, with the largest rate in the earliest stage of post-mainshock period. The magnitude of fault damage and healing varies along the rupture zone, but it is most prominent above ~7 km. Its distribution also appears to roughly correlate with the slip distribution of the 2004 earthquake [*Johanson et al.*, 2006]. The observed ratio between the *P* and *S* wave velocity changes is consistent with the opening of new fluid filled cracks at or near the time of the main shock. The results from our seismic study at Parkfield provide new information on the process of fault damage and healing on the SAF that should be forthcoming in the next cycle of the Parkfield earthquake engine.

Highly damaged fault rocks along the San Andreas Fault at Parkfield create a low velocity zone that can trap seismic waves. Observations and 3-D finite-difference simulations of the fault-zone trapped waves generated by microearthquakes at different depths and recorded at our surface dense seismic array and the seismograph installed in the SAFD mainhole at ~3 km depth show a ~200-m-wide low-velocity zone (LVZ) along the SAF reaching to depths of ~7 km or more, within which shear velocities are reduced by 20-40% in average from wall-rock velocities with the maximum velocity reduction of 40-50% in a 30-40-m-wide fault core zone, indicating the localization of severe damage on the SAF. The damage zone is not symmetric but extends farther on the southwest side of the main fault trace. The width and velocities of this zone delineated by trapped waves are confirmed by the results of the SAFOD drilling and logs that show high porosity and multiple slip planes in a ~200-m-wide LVZ across the SAF with velocity reduction of ~20-30% at ~3 km depth, within which a ~35-m-wide severely damaged zone is seen around the main slip [*Hickman et al*., 2005]. Recently, the down-hole seismic seismograph installed in the SAFOD mainhole at ~3 km depth recorded prominent fault-zone guided waves with long-duration dispersive wavetrains after both *P*- and *S*-arrivals from microearthquakes occurring below [*Ellsworth and Malin*, 2006]. We have completed a detailed examination of the waveform data recorded at the SAFOD mainhole and pilot-hole seismographs for 356 aftershocks of the 2004 Parkfield M6 earthquake. Finite-difference simulations of these waves show a ~30-40-m-wide core zone with velocities as low as 50% of the intact rocks embedded in the wider fault zone with intermediate velocity reduction, indicating that the damage zone on the SAF at Parkfield extends to the depth of at least several kilometers below 3 km, likely across the seismogenic depths in Parkfield region.

Results from our research on temporal-spatial patterns of damage on the San Andreas fault, Parkfield in 4D through this grant have produced 3 papers and reported at Conference Meetings**.** Dr. Yong-Gang Li at USC is the contact person for the reprints of these 3 papers and the ability of data acquired through this project.

PUBLICATIONS:

Li, Y. G., and P. E. Malin, San Andreas Fault damage at SAFOD viewed with fault-guided waves, *Geophys. Res. Lett.*, in review, 2007.

Li, Y. G., P. E. Malin and J. E. Vidale, Parkfield fault-zone guided waves: Low-velocity damage zone on the San Andreas fault at depth near SAFOD site at Parkfield by fault-zone trapped waves, *Scientific Drilling*, Special Issue, No. 1, doi:10.2204 /iodp.sd.s01.09, 73-77, 2007.

Li, Y. G., P. Chen, E. S. Cochran, and J. E. Vidale, Seismic velocity variations on the San Andreas Fault caused by the 2004 *M*6 Parkfield earthquake and their implications, Earth, Planets and Space, 59, 21-31, 2007.

Conference Abstracts:

Li, Y.-G., P. E. Malin, J. E. Vidale, and E. S. Cochran, High-resolution imaging of the San Andreas Fault from fault-zone trapped waves recorded at the SAFOD borehole seismograph and surface array, *EOS, Trans. Am. Geophys. Union*, T53C-04, pp168, Fall AGU Meeting, 2007.

Malin, P. E., Y.-G. Li, P. Chen, E. S. Cochran, and J. E. Vidale, Seismic Documentation for Rock Damage and Heal on the San Andreas Fault Involved in the 2004 *M*6 Parkfield Earthquake, *EOS, Trans. Am. Geophys. Union*, S43A-1048, pp74, Fall AGU Meeting, 2007.

Li, Y.-G., and P.E. Malin, Space/time property variations on the Parkfield San Andreas from fault guided waves, EarthScope National Annual Meeting, Monterey CA, March, 2007.

Li, Y.-G., J. E. Vidale, E. S. Cochran, and P. Chen, Rock damage and heal on the San Andreas Fault involved in the 2004 *M*6 Parkfield earthquake, EarthScope National Annual Meeting, Monterey, CA, March, 2007.

RESULTS:

I. San Andreas Fault damage at SAFOD viewed with fault-guided waves

Abstract Highly damaged rocks within the San Andreas fault zone at Parkfield form a low-velocity waveguide for seismic waves. Prominent fault-guided waves have been observed on the San Andreas Fault Observatory at Depth (SAFOD) seismographs, including a surface array placed across the fault-zone and a borehole unit placed in the SAFOD main hole at a depth of ~2.7 km below ground. The resulting observations are modeled here using 3-D finite-difference methods. To fit the amplitude, frequency, and travel-time characteristics of the data, the models require a downward tapering, 30-40-m wide fault-core embedded in a 100-200-m wide jacket. Compared with intact wall rocks, the core velocities are reduced by ~40% and jacket velocities by ~25%. Based on the depths of earthquakes generating guided-waves with long-duration wavetrains after the *S*-waves, we estimate that the low-velocity waveguide along the fault at the SAFOD site extends at least to depths of ~7 km. Thus it appears that significant damage zone exists at even twice the depths previously reported.

1. Introduction

Field and laboratory studies indicate that fault zones appear to undergo high, fluctuating, stresses and pervasive cracking during earthquakes [*Mooney and Ginzburg*, 1986; *Chester et al.*, 1993; *Andrews*, 2005]. However, due in part to their depth of burial, the magnitude and spatial extent of the resulting rock damages are not well constrained [*Hickman and Evans*, 1992; *Sleep et al.*, 2000]. The thickness and depth of such zones are critical ingredients in the understanding of fault mechanics [*Dieterich*; 1978; *Scholz*, 1990; *Rice*, 1992]. This article discusses these characteristics as recently observed with special fault-guided wave recordings at the San Andreas Fault Observatory at Depth (SAFOD) site near Parkfield, CA.

A zone of damaged rock surrounding the SAF at the SAFOD site has observed in previous studies using electromagnetic and seismic *P*- and *S*-wave travel time methods [*Unsworth et al*., 1997; *Thurber et al.*, 2003; *Roecker et al.*, 2004]. In these studies this zone is described as being a-little-as 200 hundred meters to as-much-as 1 km wide. The zone's observed seismic velocity reductions of 10-30% and *Vp/Vs* ratios approaching as-much-as 2.3 are thought to be caused by fracturing, brecciation, liquid-saturation, and high pore pressures. These features constitute a waveguide that traps seismic waves from earthquakes occurring within or close to it [*Li et al.*, 1990]. The amplitudes and dispersion feature of such trapped waves are known to be sensitive to the geometry and physical properties of the waveguide [*Li and Leary*, 1990; *Ben-Zion*, 1998]. At Parkfield, surface observations of fault-zone guided (trapped) waves suggest that a ~100-200-m zone of 20-40% *S*-wave velocity reduction exists to seismogenic depths [e.g. *Li et al.*, 1997, 2004a; *Malin et al.*, 1996; *Korneev et al.*, 2003]. Recently, SAFOD well logs from ~2.7 km underground have revealed a severely damaged zone around the San Andreas main fault characterized by highly fractured rock and multiple slip planes [*Hickman et al.*, 2005]. This ~200 m wide zone consists of a 30-40 m central core of ~40% lower seismic velocities surrounded by a ~25% lower velocity jacket inferred by fault guided PSV waves recorded at the seismograph installed in the SAFOD main hole at depth [*Ellsworth and Malin*, 2006].

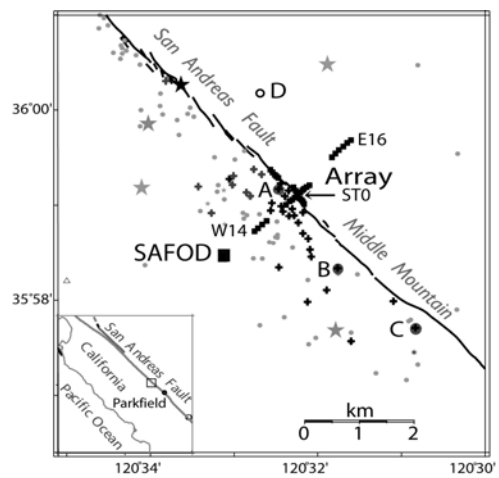

Figure 1 Locations of the study area (box in inset map), 45 portable seismographs (small squares) across and along the SAF near the SAFOD site (square), explosions (stars); and 120 microearthquakes (dots) recorded in the fall of 2003. Station ST0 of the array was located on the SAF surface trace; W14 and E16 on its west and east sides. Crosses denote 33 events generating fault-guided waves used in Fig. 4. Event A (solid circle), the SAFOD drilling target, occurred at ~2.7 km depth in 2003; its waveforms shown in Fig. 2c. Event B, a ~7 km deep aftershock of the 2004 *M*6 Parkfield earthquake, was recorded at the SAFOD main hole seismograph installed at ~2.7 km depth in 2005; its waveforms shown in Fig. 2d. Events C and D (solid and open circles) were deeper at 11 and 9 km, and were recorded on the surface array in 2003; their waveforms shown in Fig. 3.

2. Data and results

In fall 2003, as part of a site characterization program, an array of 45 portable seismographs was deployed across and along the surface trace of the SAF near SAFOD site [*Li et al.*, 2004b] (Fig. 1). About 120 local earthquakes were recorded at this surface array, including 33 events showing clear guide waves at depths between 2 and 12 km, from which the raypath incidence angles to ST0 are smaller than 30° from vertical. In December of 2004 and later a borehole seismograph was installed in the SAFOD mail hole at ~2.7 km depths where the SAF is characterized by a highly fractured and low velocity zone [*Ellsworth and Malin*, 2006] (Fig. 2a, b). Fig. 2c, d illustrate representative surface seismograms recorded at the surface array for a ~2.7 km-deep event (the SAFOD drilling target) in 2003 and borehole seismograms for a ~7 km-deep

aftershock of the 2004 M6 Parkfield earthquake, showing the prominent fault guided waves which are simulated using the model in Fig. 2a.

Figure 3 shows 3-component seismograms recorded at the surface array in 2003 for 2 other representative earthquakes: events C and D of Fig. 1. The primary focuses here on these events are their relative relationships in terms Of event location and recording points versus the types of waves generated and what these imply for the velocity structure of the SAF at SAFOD. There are two major points to be made in this regard, both illustrated more details in Fig. 4. The first point to be made is that the events whose locations and observation points appear closest to the projected trace of the SAF generate prominent fault guided waves characterized by relatively large amplitudes and long wavetrains following *S*-waves. The second point is that the time dispersion of the latter signals after *S*-waves is a strong function of event depth. Taken together, these two characteristics imply that the guided waves were traveling along a relatively continuous channel connecting the events and observation points.

These relations and the fault zone characteristics they imply were investigated further using a 3-D finite-difference waveform modeling code [*Graves*, 1996]. In this study, only the *S*-velocity related fault-zone trapped waves (FZTWs) were emphasized in the model computation. The study area was covered with a 10 m grid of computation point. A double-couple source is used for earthquakes while a point source used for explosions. The fault zone and surrounding rock velocity and attenuation in the model used for these simulations was built in several steps.

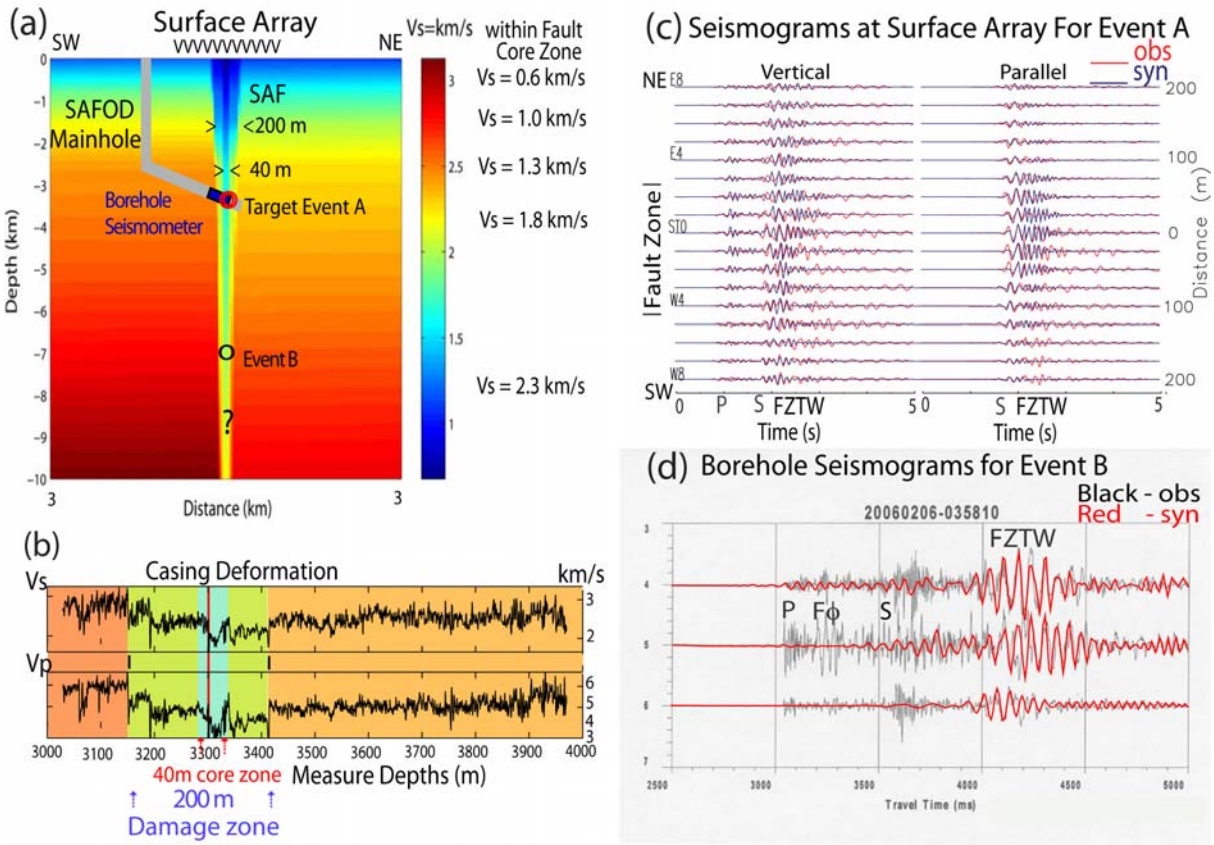

Figure 2 (a) Cross section near the SAFOD site showing the *S*-wave velocity model used in this study to compute synthetic fault-zone trapped waves (FZTWs) for the surface and borehole observations recorded in 2003 and 2005. Earthquakes A and B illustrate this type of fault guided waves used in this study. (b) Seismic velocities from SAFOD well logs showing the 40-m fault core and 200 m jacket low velocity damage zones. The red line indicates the location where fault creep is deforming the borehole casing. (c) Observed (red) and computed (blue) vertical- and parallel-component seismograms at the surface array for event A. The seismograms were low-pass filtered below 8 Hz and are plotted using a single global scale. (d) Observed and computed 3-component borehole seismograms recorded for event B. The synthetic seismograms have been low pass filtered below 12 Hz. The large signal between the P- and S- waves labeled $\mathbf{F_\phi}$ has been recently identified as a fault guided P-wave [*Malin et al.*, 2006; *Ellsworth and Malin*, 2006].

First, the direct and guided waves from explosions shown in Fig. 1 were modeled to obtain a velocity model for the upper 2 km of the SAFOD site and the shallow structure of the SAF as we did for modeling the FZTWs recorded in our previous experiment conducted near Parkfield [*Li et al.*, 2004a]. Then, using the well log velocities and 2005 borehole seismogram as calibration points, progressively deeper earthquakes with prominent guided waves were modeled by adjusting the fault structure immediately above their hypocenters. The velocities in surrounding rocks are constrained by tomography profiles obtained at Parkfield

[*Thurber et al.*, 2003; *Roecker et al.*, 2004]. The result of this process is the downward tapered, two-layer, low-velocity fault zone sandwiched between different east and west sides of the SAF (Fig. 2a.). The waveform fits corresponding to this velocity model are shown in Fig. 2c, d. The synthetic seismograms fit amplitude behaviors and traveltimes of the FZTWs recorded at both the borehole seismograph and surface array stations within the fault zone as well as those east and west of the SAF. They also fit the depth dependant dispersion characteristics of both the on-fault and off-fault source-receiver relations seen in the data (Fig. 4c). We tested a shallow fault zone truncated at 4 km depth in modeling for the 11 on-fault events. Fig. 4d illustrates the synthetic seismograms showing nearly the same wavetrain length of FZTWs after the *S*-waves for events below 4 km and shorter than those seen in Fig. 4c.

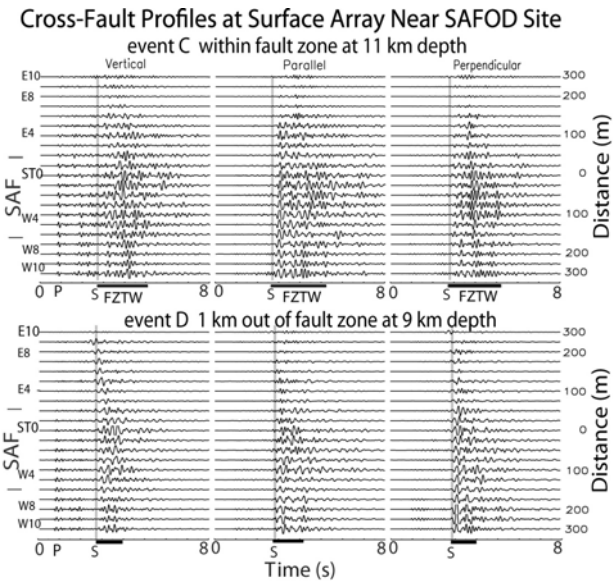

Figure 3 Three-component seismograms for events C and D. These representative seismograms were low-pass filtered below 6 Hz, aligned on the *S*-waves, and plotted with fixed amplitude scales for all traces in each plot. Fault-zone trapped waves (FZTW) with large amplitudes and long wavetrains after the S-arrivals are seen on the stations near the SAF surface trace at ST0 for the on-fault event C but not for the off-fault event D.

Evidently, the SAFOD site guided waves can be explained in terms of a tapered, 30-40 m wide fault core of ~40% reduced velocity inside of a wider 100-200 m jacket of ~25% reduced velocity. The relatively intact rocks surrounding this composite damage zone have different velocities east and west of the SAF. Further, based on successful matching of the dispersion characteristics of the FZTWs following the *S*-waves as a function of depth, it would appear that, at least the low velocity jacket, and possibly its interior core, extends downward to no less than ~7 km (Fig. 4c). This is the depth inferred by the most clearly resolved and best fit guided waves seen in the SAFOD borehole seismograms [*Ellsworth and Malin*, 2006] that are modeled here (Fig. 2d).

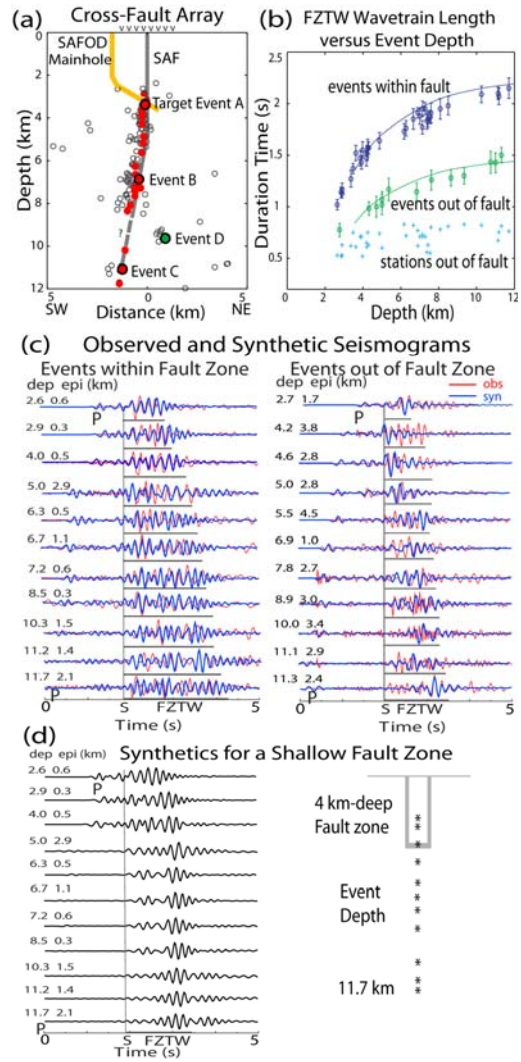

Figure 4 (a) Cross section through the SAF (grey line) at the SAFOD site showing locations of the microearthquakes (circles) with their epicenters shown in Fig. 1. Red circles mark 33 events showing strong fault-zone trapped waves (FZTW). Their epicenters are marked by crosses in Fig. 1. The locations of events A-D are also shown. (b) The measured time durations (denoted by blue circles) of FZTWs after *S* waves at stations within the fault zone for 33 on-fault earthquakes versus event depth, compared to those (green circles) measured at the same stations for off-fault earthquakes and those (blue crosses) at stations away from the fault zone for on- and off-fault events. Each data point is the average of 4 on- or off-fault stations. The error bars are standard deviations and the curves are polynomial fits to the data. (c) Observed and synthetic vertical-component seismograms at station ST0 for 11 on-fault and 11 off-fault earthquakes at different depths. *S*-arrivals for these events are aligned at the same time. The focal depth and epicentral distance from ST0 are plotted for each event. The finite-difference synthetic seismograms are computed using the model in Fig. 2a. Seismograms have been <8 Hz filtered and are plotted in trace-normalized. Bars denote the post-*S* wave durations, in which amplitude envelopes of FZTWs are above twice level in later coda. (d) Synthetic seismograms at ST0 for 11 on-fault events using a 4-km-deep fault zone.

3. Discussions and Conclusions

The damage zone at seismogenic depths may be caused by intense fracturing during earthquakes, including brecciation. Alternatively, given the fluid leakages currently taking place into the SAFOD well, the cause might relate to liquid-saturation and high pore-fluid pressure nears the fault. However, pore fluids arising from depth appear to hold a complex relationship with this damage zone, with its outer portions appearing to be more permeable than its core [Lockner et al., 2000]. Moreover, the damage zone may actually form more of a fluid barrier which fluids are simply pounded against. The damage zone is also asymmetric, apparently broader on the southwest side of the main fault trace. The asymmetry may imply that the fault has a moving damage zone or that when it ruptures it may preferentially damage the already weakened rocks [*Chester et al.*, 1993]. Alternately, greater damage may be inflicted in the extensional quadrant than the compressional quadrant near the propagating crack tip [*Andrews*, 2005]. Although the structural model shown in Fig. 2a accounts for the FZTWs and $\mathbf{F_\phi}$ observations and its parameters at ~3 km depth are confirmed by logging data, it is likely to represent a gross average of the actual fault-zone structure. The true structure in 3-D will certainly be more complicated, and the damage magnitude and extent will vary along the fault strike and depth due to rupture distributions and stress variations over multiple length and time scales.

References

Andrews, D. J. (2005), Rupture dynamics with energy loss outside the slip zone, *J. Geophys. Res.*, *110*, B01307, dio: 0.1029.

Ben-Zion, Y. (1998), Properties of seismic fault zone waves and their utility for imaging low-velocity structure, *J. Geophys. Res*., *103*, 12,567–12,585.

Chester F., Evans, J. and R. Biegel (1993), Internal structure and weakening mechanisms of the San Andreas fault, *J. Geophys. Res*., *98*, 771-786.

Dieterich, J. H. (1978), Time-dependent friction and the mechanics of strike-slip, *Pure Appl. Geophys*., *116*, 790-806.

Ellsworth, W. L., and P. E. Malin (2006), A first observation of fault-guided PSV-waves at SAFOD and its implications for fault characteristics, *EOS, Transactions, and American Geophysics Union*, *87*, T23E-02, p154.

Graves, R. W. (1996), Simulating seismic wave propagation in 3D elastic media using staggered-grid finite differences, *Bull. Seism. Soc. Am*., *86*, 1091-1106.

Hickman, S. H., and B. Evans (1992), Growth of grain contacts in halite by solution-transfer: Implications for diagenesis, lithification, and strength recovery, in *Fault Mechanics and Transport Properties of Rocks*, pp. 253-280, Academic, San Diego, Cal.

Hickman, S. H., M. D. Zoback, and W. L. Ellsworth (2005), Structure and Composition of the San Andreas fault zone at Parkfield: Initial results from SAFOD Phase 1 and 2, *EOS, Transactions, and American Geophysics Union*, *83*, No.47, p237.

Korneev, V. A., R. M. Nadeau, and T. V. McEvilly (2003), Seismological studies at Parkfield IX: Fault-zone imaging using guided wave attenuation, *Bull. Seism. Soc. Am. 80*, 1245-1271.

Li, Y. G., P. Leary, K. Aki, and P. Malin (1990), Seismic trapped modes in Oroville and San Andreas fault zones, *Science*, *249*, 763-766.

Li, Y. G. and P. C. Leary (1990), Fault zone trapped seismic waves, *Bull. Seism. Soc. Am.*, 80, 1245-1271.

Li, Y. G., W. Ellsworth, C. Thurber, P. Malin, and K. Aki (1997), Observations of fault-zone trapped waves excited by explosions at the San Andreas fault California, *Bull. Seism. Soc. Am. 87*, 210-221.

Li, Y. G., J. E. Vidale, and E. S. Cochran (2004a), Low-velocity damaged structure on the San Andreas fault at Parkfield from fault-zone trapped waves, *Geophys. Res. Lett. 31*, L12S06, p1-5.

Li, Y. G., E. S. Cochran, and J. E. Vidale (2004b), Low-velocity damaged structure on the San Andreas Fault at seismogenic depths near the SAFOD drilling site, Parkfield, CA from fault-zone trapped waves, *EOS, Transactions, and American Geophysics Union*, *85*, No. 47, F1313.

Lockner, D., H. Naka, H. Tanaka, H. Ito, and R. Ikeda (2000), Permeability and strength of core samples from the Nojima fault of the 1995 Kobe earthquake, *USGS Open file, Report* 00-129, 147-152.

Malin, P. E. M. Lou, and J. A. Rial (1996), $\mathbf{F_R}$ waves: A second fault-guided mode with implications for fault property studies, *Geophysical Research Letters*, *23*, 3547 – 3550.

Malin, P. M., E. Shalev, H. Balven, and C. Lewis-Kenedi (2006), Structure of the San Andreas Fault at SAFOD from P-wave tomography and fault-guided wave mapping,, *Geophys. Res. Letter 33*, No. 13, pp. 13314, 2006GL025973.

Mooney, W. D. and A. Ginzburg (1986), Seismic measurements of the internal properties of fault zones, *Pure Appl. Geophys. 124*, 141-157.

Rice, J. R. (1992), Fault stress states, pore pressure distributions, and the weakness of the San Andreas fault, in *Fault Mechanics and Transport Properties of Rocks*, edited by B. Evans and T.-F. Wong, 475-503, Academic, San Diego, Calif.

Roecker, S., C. Thurber, and D. McPhee (2004), Joint inversion of gravity and arrival times data from Parkfield: New constraints on structure and hypocenter locations near the SAFOD drill site, *Geophys. Res. Lett., 31*, DOI 10.1029/2003GL019396.

Scholz, C. H. (1990), *The Mechanics of Earthquakes and Faulting*, Cambridge Univ. Press, New York.

Sleep, N. H., E., Richardson, and C. Marone (2000) Physics of friction and strain rate localization in synthetic fault gouge, *J. Geophys. Res. 105*, 25,875-25,890.

Thurber, C., S. Roecker, K. Roberts, M., Gold, L. Powell, and K., Rittger (2003), Earthquake location and 3-D fault zone structure along the creeping section of the San Andreas fault near Parkfield, CA: Preparing for SAFOD, *Geophys. Res. Lett*. ***30***, 1112-1115.

Unsworth, M., P. Malin, G. Egbert, and J. Booker (1997), Internal structure of San Andreas fault at Parkfield, CA, *Geology*, 356-362.

In order to further examine the depth extension of the low-velocity damage zone on the SAF Parkfield, we have analyzed the data recorded at the SAFOD borehole seismographs for ~350 aftershocks of the 2004 *M*6 Parkfield earthquake, occurring at different depths and epicentral distances along the fault strike (Fig. 5a, c).The waveform data are provided by SAFOD Program through the research team led by Peter Malin at Duke University. We observed prominent fault-zone trapped waves (FZTWs) at the seismograph installed in the mainhole at ~3 km depth, where the San Andreas Fault passes, for aftershocks occurring within the fault zone below the borehole (Fig. 5b). The trapped waves are characterized by relatively large amplitudes and low frequencies with long wavetrains after *S*-waves. However, such type of waveforms were not registered at the seismograph installed in the SAFOD pilot hole, 1.8 km away from the SAF, for the same aftershocks. We note that the length of FZTW duration after the S-arrival increases as the travel distance increases along the fault strike and with the depth. Observations and 3-D finite-difference modeling of these FZTWs show that the low-velocity waveguide (fault damage zone) on the SAF likely extends across seismogenic depths at least 7-8 km.

Figure 5d show the waveforms recorded at the SAFOD mainhole and pilot-hole seismographs for 5 clustered aftershocks in group 4 occurring within the fault zone at ~10.5-km depth and ~15-km SE of the SAFOD site. The FZTWs with long-duration (~2 s) and low-frequency (5-10 Hz) appeared after *S*-arrivals in the mainhole seismograms while brief body waves at high frequencies appeared in the pilot-hole seismograms for the same events. These observations indicate the existence of a low-velocity waveguide along the SAF at depth between the events and mainhole seismograph.

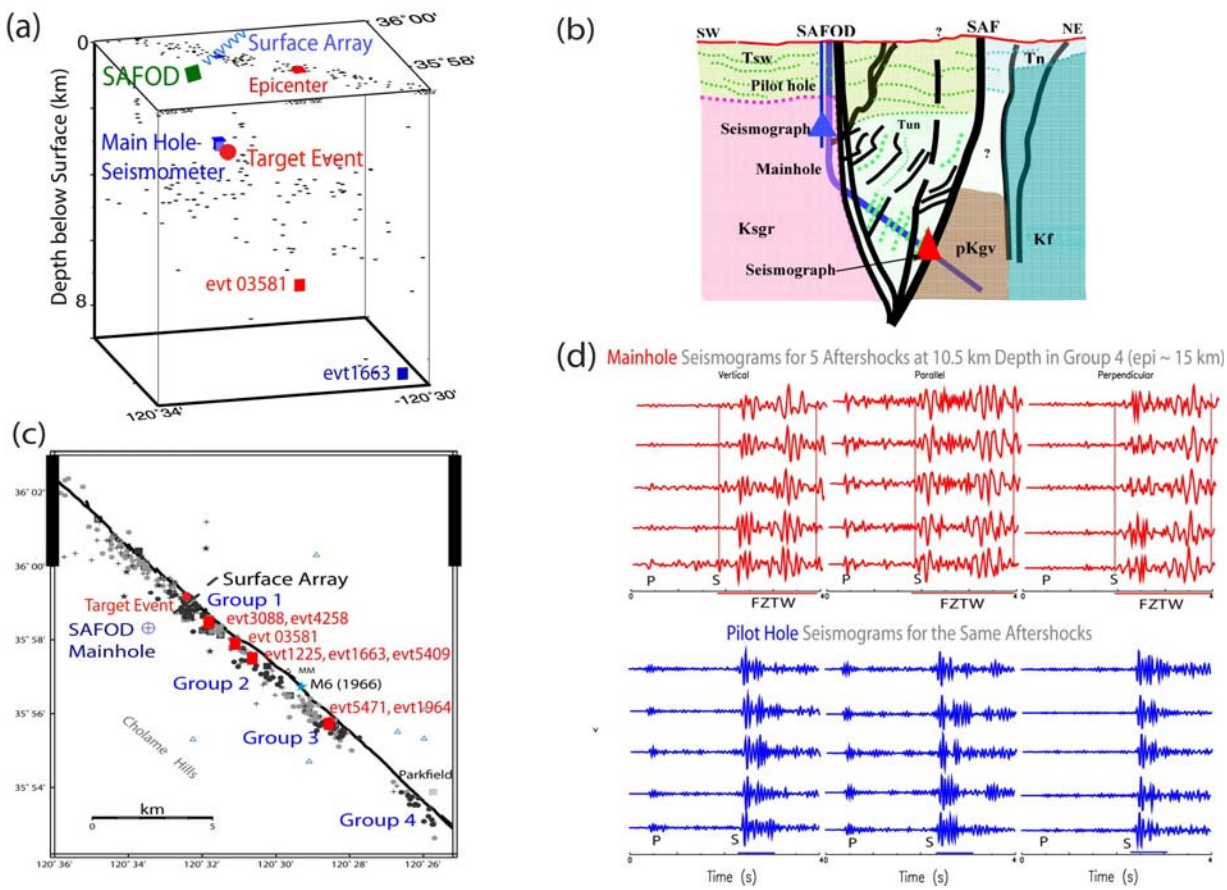

Figure 5 (a) 3-D view of locations of aftershocks (black dots) of the 2004 M6 Parkfield earthquake recorded at the SAFOD Main Hole seismograph (blue box) that was installed at the depth of ~3 km. (b) SW-NE cross section along the Phase 2 SAFOD Main Hole toward the surface trace of the SAF. The borehole seismographs installed in the SAFOD mainhole and pilot hole (denoted by red and blue triangles). The geological interpretation is based on the results of a Drill Bit Seismic reflection profile gathered during the 2004 Phase 1 drilling [Ellsworth and Malin, 2006]. (c) Map view shows aftershocks recorded at SAFOD borehole seismographs in 2004 and 2005. (d) 3-component seismograms recorded at SAFOD mainhole and pilot hole seismographs for 5 on-fault aftershocks of the 2004 M6 Parkfield earthquake show prominent fault-zone trapped waves (FZTW) with large amplitudes and long wavetrains after S-waves at the mainhole seismograph located within the fault zone but not at the pilot-hole seismograph 1.8 km away from the fault, indicating a low-velocity waveguide (damage zone) existing along the SAF at depth between the mainhole seismograph and the events.

In Figure 6, we illustrate more examples of seismograms recorded at SAFOD mainhole and pilot-hole seismographs for aftershocks occurring within the fault zone at different depths and epicentral distances. Again, we observe prominent fault-zone trapped waves in mainhole seismograms but not in pilot-hole seismograms for these events. We also note that the time duration of FZTWs after *S*-arrivals increases as the travel distance of the event increases along the fault strike ad with depth, indicating a roughly continuous low-velocity waveguide extends along the Parkfield San Andreas fault and with depth to at least 7-8 km.

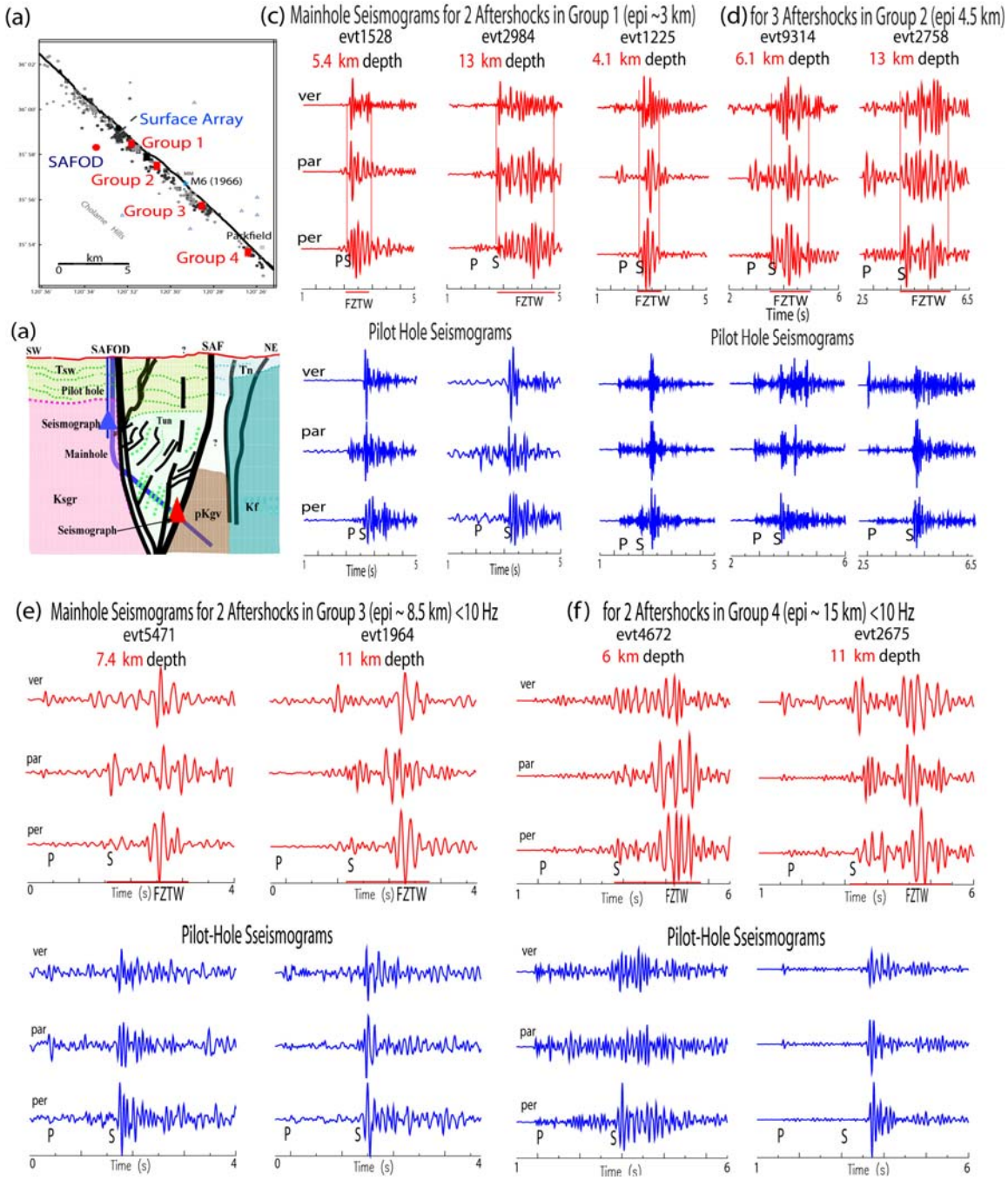

Figure 6 (a) and (b) as the same in Fig.5 a, b. (c)-(f) 3-component seismograms recorded at SAFOD mainhole and pilot hole seismographs for on-fault aftershocks in group 1-4 at different depths and distances from SAFOD site show prominent fault-zone trapped waves (FZTW) with large amplitudes and long wavetrains after S-waves in the mainhole seismograms but not at in pilot-hole seismograms, indicating a low-velocity waveguide (damage zone) existing along the SAF at depth between the mainhole seismograph and these events.

In order to further examine the depth extension of the low-velocity zone on the SAF, we used the data from the aftershocks in groups 1 and 2 located within the fault zone at different depths with the raypath incidence angles to the SAFOD site smaller than 30° from vertical (Fig. 7a). Figure 7b shows seismograms recorded at the mainhole seismograph for 9 on-fault events. The time duration of fault-zone trapped wavetrains following *S*-arrivals progressively increases from ~0.5 s to ~1.8 s as the event depths increase from 3.8 km to 13 km. In contrast, much shorter wavetrains after *S*-arrivals with flat changes in duration are registered at the pilot-hole seismograph for the same events. Figure 7c shows the measured wavetrain lengths of FZTWs recorded at the SAFOD borehole seismographs for these events, indicating that the low-velocity waveguide formed by the damage rocks of the SAF likely extends across seismogenic depths in the upper crust at Parkfield. The data from the aftershocks along the rupture zone of the 2004 *M*6 Parkfield earthquake also show that the LVZ extends continuously along the SAF strike in the Parkfield region (Fig. 7d).

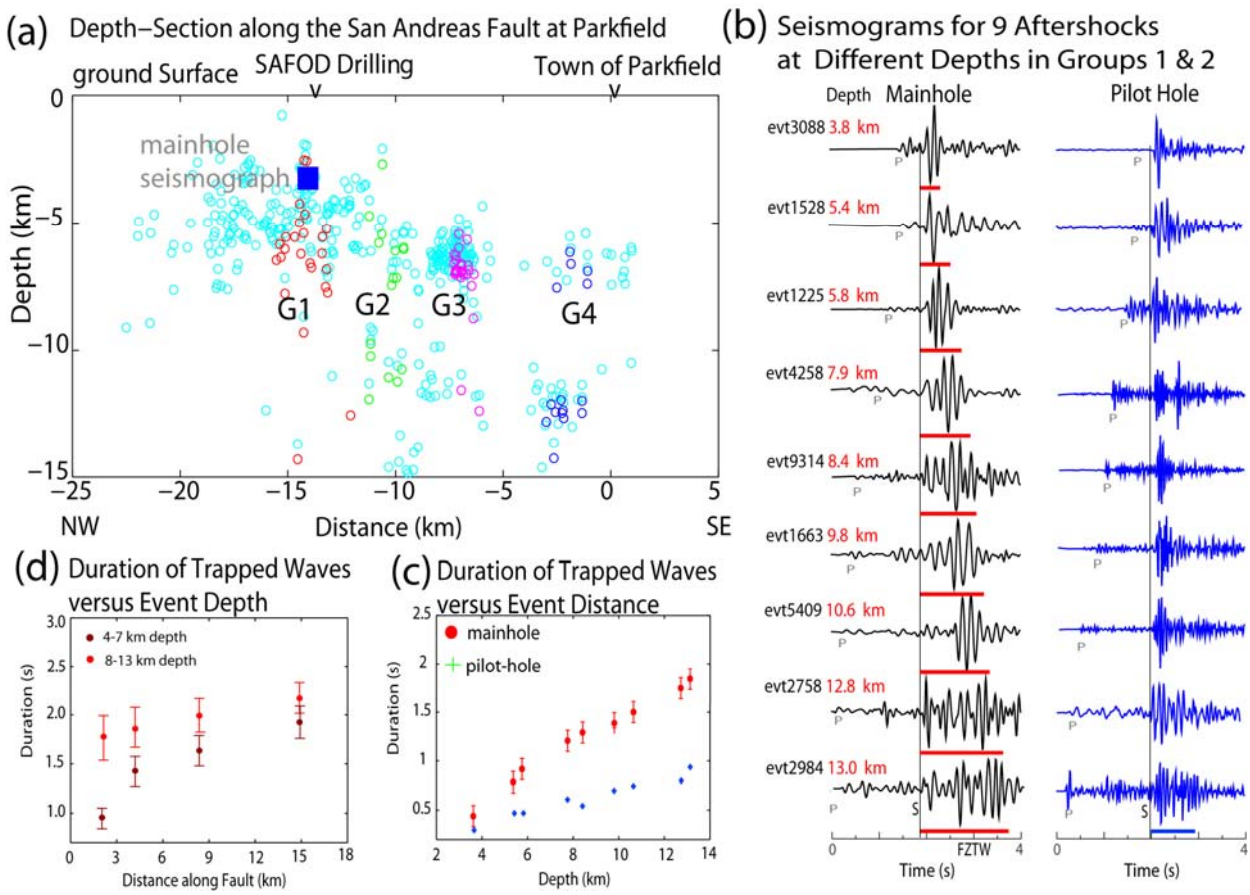

Figure 7 (a) Vertical section along the SAF near the SAFOD site shows locations of ~350 aftershocks (circles) of the 2004 *M*6 Parkfield earthquake recorded at the borehole seismograph (blue square) installed in the SAFOD mainhole at ~3 km depth. Four groups (G1-G4) of aftershocks include events with the epicentral distances of ~2 km, 4.5 km, 8.5 km and 15 km from the SAFOD site. (b) Left: Vertical-component seismograms recorded at SAFOD mainhole seismograph for 9 on-fault aftershocks in group G1 and G2 at different depths show an increase in time duration (denoted by the red bar) of FZTWs as event depths increase. The incidence angles of raypaths from these events to the mainhole seismograph are smaller than 30° to vertical. *S*-arrivals for these events are aligned at the same time. Right: Seismograms recorded at the SAFOD pilot-hole seismograph for the same events show much shorter FZTW wavetrains and flat changes with event depths. (c) The measured time durations of FZTWs after *S*-arrivals in mainhole (red) and pilot-hole (blue) seismograms versus focal depths for 9 on-fault aftershocks in Fig. 7b. Each data point is averaged from measurements of 3 components for the event. Error bars are standard deviations. (d) The measured time durations of FZTWs after *S*-arrivals in mainhole seismograms for aftershocks in 4 groups versus epicentral distances from SAFOD site (see Fig. 7a). Each data point is averaged from measurements for the events in G1-G4, respectively. Red (violet) denotes the data from events at depths of 4-7 km (8-13 km). Error bars are standard deviations.

Based on our observations of fault-zone trapped waves at the surface array and borehole seismograph in the SAFOD mainhole, we construct a velocity and *Q* model across the SAF near the SAFOD site as shown in Fig. 8a. The wall-rock velocities are constrained by tomography profiles at Parkfield [*Thurber et al.*, 2003; *Roecker et al.*, 2003]. Using a 3-D FD code [*Graves*, 1996], we simulate FZTWs generated by explosions and shallow earthquakes and recorded at the surface array to determine the fault zone structure at depths above 3-km. Then, we simulate trapped waves from deep earthquakes and recorded at the manhole seismograph to obtain a model of the SAF with depth-variable structure at seismogenic depths as shown in Fig. 8b. The width and velocities of the damage zone at 3 km depth in this model are constrained by the logging measurements in the SAFOD mainhole (Fig. 2b) [*Hickman et al*., 2005]. For examples, Figs. 8c-8e exhibit 3-D finite-difference synthetic seismograms for aftershocks in groups 1-4 occurring within the fault zone at different depths and epicentral distances from the SAFOD mainhole seismograph. We obtained a good fit of synthetics to observations, showing that this model is applicable for interpretation of the damage structure on the Parkfield SAF at seismogenic depths.

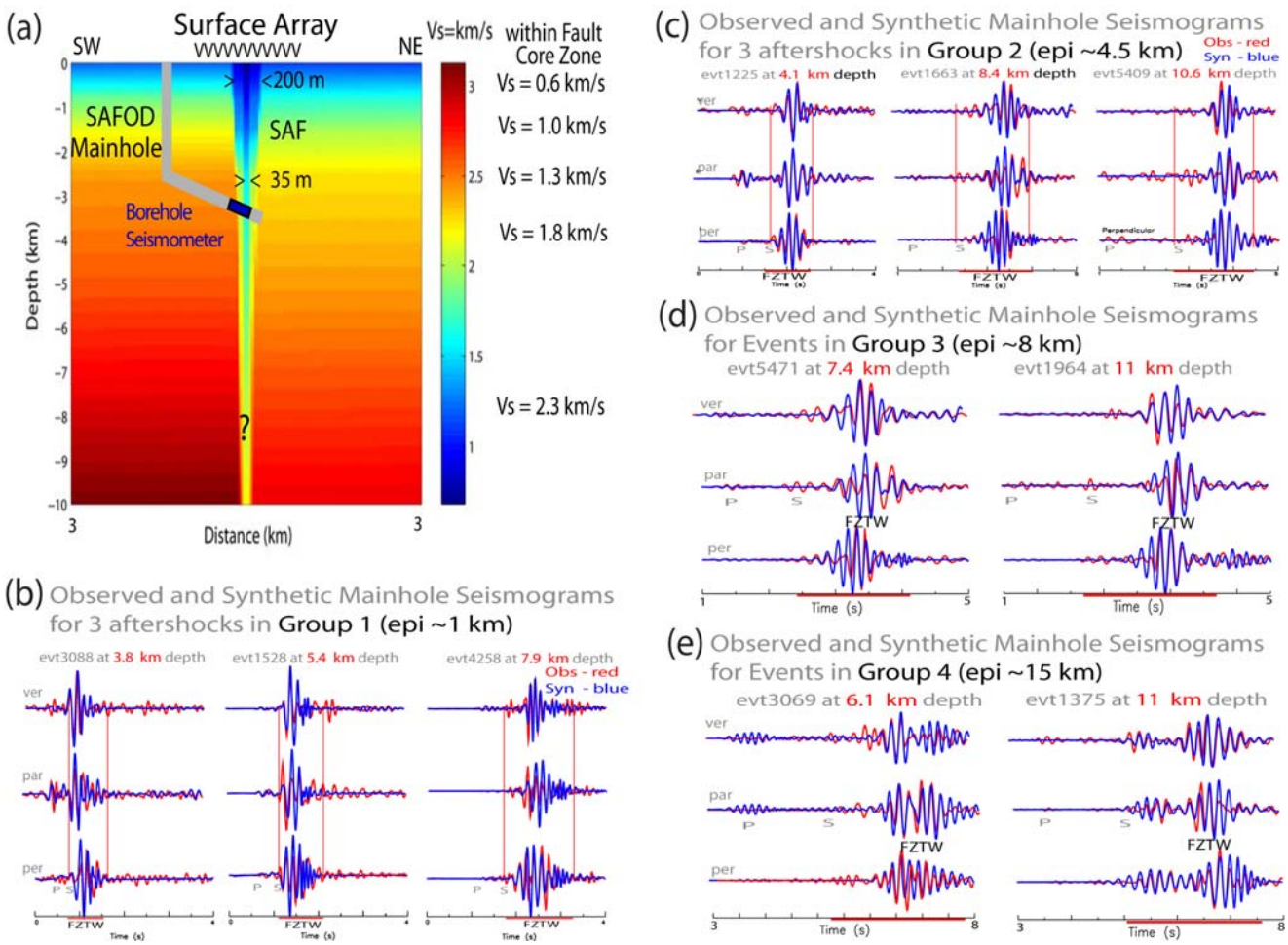

Figure 8 (a) Cross section near the SAFOD site showing the *S*-wave velocity and *Q* value model used in this study. (c)-(e) Observed and 3-D finite-difference seismograms at SAFOD mainhole seismograph for Parkfield aftershocks occurring within the fault zone at different depths and epicentral distances show prominent fault-zone guided waves, the wavetrain length of which increases as the travel distance increases along the fault strike or with the depth, suggesting a continuous low-velocity damage zone on the SAF extending across seismogenic depths. The model in Fig. 8a is used for complete FD waveform computation. A double-couple source is used for aftershocks.

II. Seismic Evidence for Rock Damage and Healing on the San Andreas Fault Associated with the 2004 *M*6 Parkfield Earthquake

Results from the data recorded at the surface seismic array

The *M*6 Parkfield earthquake that occurred on 28 September 2004 provides us a rare opportunity to examine the possible variations in the volume and magnitude of the low-velocity anomalies on the SAF over the earthquake cycle. After this earthquake, we deployed a dense seismic array at the same sites as used in our experiment in the fall of 2002. The data recorded for repeated explosions detonated within the San Andreas in 2002 and after the 2004 *M*6 Parkfield earthquake show a few percent decreases in seismic wave velocity within an ~200-m-wide zone along the fault strike at the shallow depth, most likely due to the co-seismic damage of rocks during dynamic rupture in this *M*6 mainshock [*Li et al.*, 2006]. The data from clustered aftershocks at the depth to 7 km show velocity recovery by ~1.2% within the fault zone in 3 months after the mainshock, indicating that the damaged rock has been healing following the mainshock. The width (~200 m) of the damage zone characterized by larger velocity changes is consistent with the low-velocity waveguide model on the San Andreas fault near Parkfield derived from fault-zone trapped waves [*Li et al.*, 1997, 2004; *Korneev et al.*, 2003]. The damage zone is not symmetric, instead extending farther on the southwest side of the main fault trace. The healing rate was not constant but largest in the earliest stage of post-mainshock. The magnitude of fault damage and healing varies across and along the rupture zone, indicating that the greater damage was inflicted and thus greater healing is observed in regions with larger slip in the mainshock. Observations of rock damage during the mainshock and healing soon thereafter are consistent with our interpretation of the low-velocity waveguide on the SAF being at least partially softened in the 2004 *M*6 mainshock, with additional cumulative effects due to recurrent rupture.

The large amount of aftershock data recorded at our FZ array deployed in the middle of a high-slip part of the surface rupture in the 2004 Parkfield earthquake and co-sited in our experiment conducted in the fall of 2002 provide us a good opportunity to study co-seismic rock damage and post-mainshock fault healing associated with this *M*6 earthquake (Fig. 1a). We recorded the data from ~1000 aftershocks in ~4 months starting from 1 week after the mainshock. We also detonated 2 explosions within the fault zone near Parkfield about 3 months after the mainshock. Shot PMM in Middle Mountain was a repeated explosion of the shot in the fall of 2002. We examined the data from repeated explosions and similar aftershocks recorded at our seismic arrays deployed at the SAF, Parkfield in 2002 and 2004 for study of spatial and temporal changes in fault zone properties associated with this *M*6 earthquake. Fig. 1b shows similar waveforms recorded at stations of the cross-fault array for repeated shot PMM. We measured traveltime delays using moving-window waveform cross-correlation method for each pair of recordings for repeated shots, showing larger changes within a ~200-m-wide fault zone. The width of the damage zone characterized by larger velocity changes is in general consistent with the low-velocity waveguide model on the SAF at Parkfield derived from fault-zone trapped waves [*Li et al.*, 2004]. We estimate that the *P* wave velocity decreased by ~1.5% and the *S* wave velocity decreased by ~1.2%. Guided waves with longer travel times had larger time advances, again resulting in ~1.2% increase in velocity within the rupture zone in the time period between the two repeated shots. In contrast, the *S*-wave velocity decreased by less ~0.5% in the surrounding rocks. Assuming that there were no significant changes in seismic velocity after the fall of 2002 and before 28 September, 2004 at Parkfield region [*Rubinstein and Beroza*, 2005], the measured velocity decreases between 2002 and 2004 are most likely caused by the co-seismic rock damage with crack opening due to the latest *M*6 Parkfield earthquake. Note that the moderate velocity decrease on the north fault strand. The north fault strand might have experienced minor breaks due to secondary slip and strong shaking from ruptures on the main fault in the *M*6 earthquake. We have estimated the degree of fluid saturation in cracks from the ratio between *P*-wave and *S*-wave traveltime changes ($\Delta tp/\Delta ts$) using equations for the elastic moduli of the medium with isotropically oriented penny-shaped cracks [*Garbin and Knopoff*, 1975] as we studied the fault healing on rupture zones of the 1992 Landers and 1999 Hector Mine earthquakes [*Li et al.*, 1998; 2003], showing 0.57 of $\Delta tp/\Delta ts$ within the fault zone but ~0.65 out of the zone, indicating more water contained in cracks at shallow depth. Fig. 1c shows seismograms recorded at array A for a *M*1.3 local earthquake occurring on Julian date R291 in 2002 within the fault zone at depth of ~6.5 km beneath Middle Mountain and its repeated event occurring on R288 in 2004, ~2 weeks after the *M*6 Parkfield earthquake on Julian date R275. Moving-window cross-correlations of waveforms show that seismic waves

traveled slower in 2004 than in 2002, indicating a maximum of ~2.3% reduction in shear velocity within the fault zone at seismogenic depth, most likely caused by the co-seismic damage of rocks due to the *M*6 mainshock.

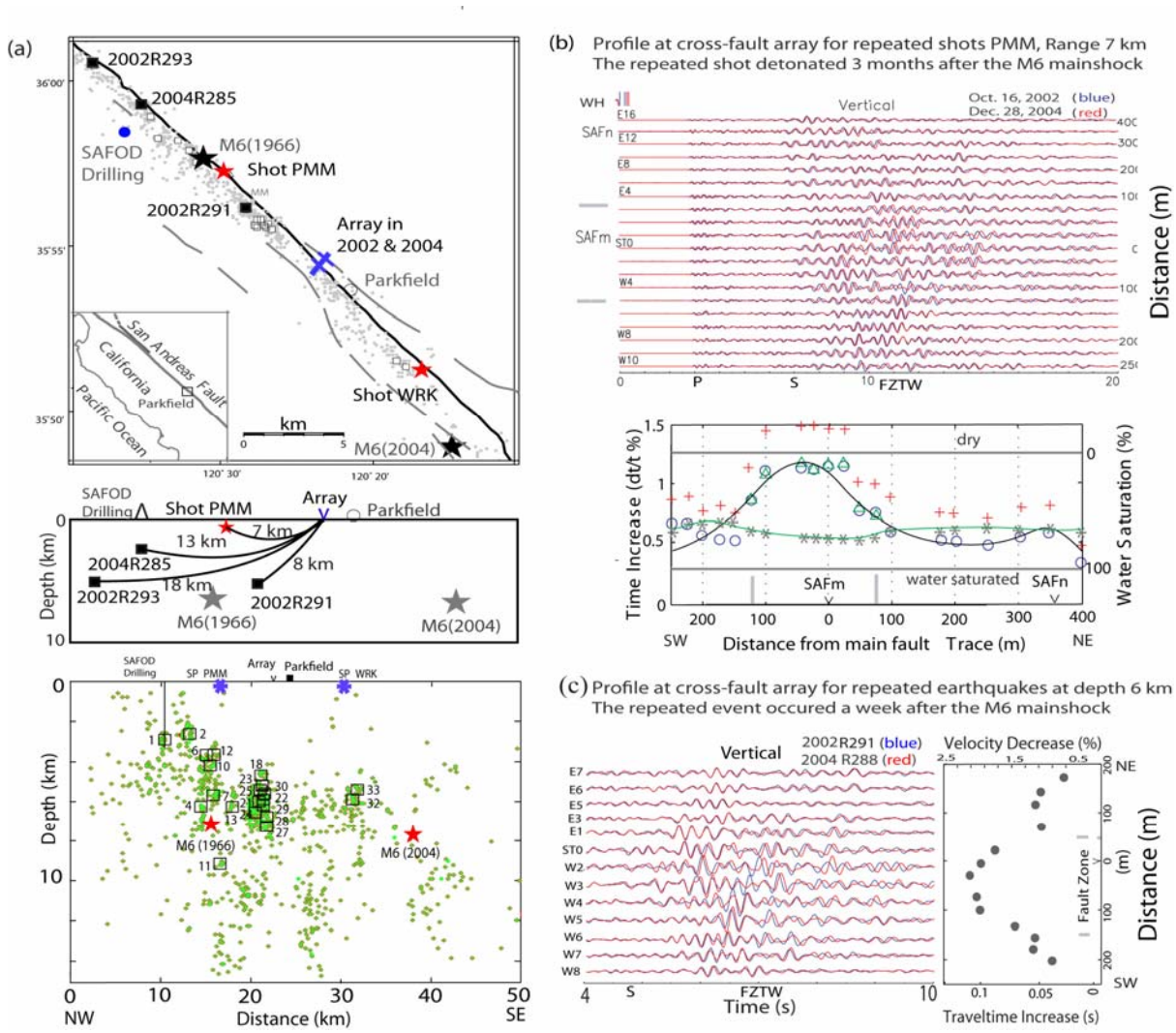

Figure 1 (a) Top: Map shows locations of seismic arrays (blue lines) deployed across and along the SAF main fault and north strand near Parkfield in 2002 and 2004, and shots PMM and WRK. Dots denote aftershocks recorded at our array in 2004. Open squares – 21 clusters of repeated aftershocks used to examine fault healing. Solid squares - earthquakes recorded on Julian date R291 and R293 in 2002 and their repeated events in 2004. Stations ST0 and E15 were located on the main fault and north strand. Each cluster includes at least 5 similar aftershocks located within 200 m. (b) Top: Vertical-component seismograms recorded at cross-fault array for repeated shot PMM before and after the 2004 M6 Parkfield earthquake. The shot origin time is at 0 s. WH denotes the wellhead station; the unclipped first P arrivals show identical arrival times for the repeated shots, but seismic waves traveled slower after the 2004 M6 mainshock. Bottom: Traveltime increases for P (red crosses), S (blue circles), and trapped waves (green circles) measured by moving-window waveform cross-correlations at working stations across the SAF for repeated shot PMM, showing seismic velocity decreased after the M6 mainshock. The blue curve fits to traveltime increases of S waves in 2004. A pair of vertical grey bars denotes a ~200-m-wide zone with greater travel time increases. Ratio of traveltime changes for P to S waves (green stars with a curve) indicates the degree of water saturation in cracks. Two horizontal lines indicate a range of water percentage for Poisson solid. (c) Left: Seismograms at the cross-fault array for two repeated micro-earthquakes before and after the 2004 M6 Parkfield earthquake. The P-wave arrivals are aligned and the seismograms have been <5 Hz filtered Right: The maximum S-traveltime increases of seismic waves in the 2-10 s windows across the SAF. The increases were measured by waveform cross-correlations between the 2002 and 2004 events.

We also found that the damage zone is asymmetric, broader on the southwest side of the main fault trace. The asymmetry may imply that the fault zone has a significant cumulative damage due to previous large earthquakes on the SAF. When a fault ruptures, it may preferentially damage the already weakened rocks in the zone, even though those rocks are not symmetrically distributed on either side of the main slip plane [*Chester et al.*, 1993]. Alternately, greater damage may be inflicted in the extensional quadrant than the compressional quadrant near the propagating crack tip [*Andrews*, 2005].

Fig. 2a shows seismograms recorded at station W1 within the fault zone for the event on R291 in 2002 and its 10 repeated events occurring between R281 and R360 in 2004, ~1 week to ~3 months after the 2004 *M*6 earthquake. Moving window measurements of traveltimes of seismic waves show the largest delay of ~125 ms in the late coda plus the change of *P*-wave between the earliest aftershock we recorded on R281 in 2004 and the event on R291 in 2002, and then gradually decreased to ~55 ms for the later repeated event on R350 (Fig. 2b). We estimate that the apparent shear velocity within fault zone decreased by ~2.5% between R291 in 2002 and R281 in 2004, and then increased by ~1.2% in the following ~3 months, indicating that fault-zone rock has been damaged with shear velocity reduced by at least 2.5% in dynamic rupture of the 2004 *M*6 mainshock and being healing with rigidity recovery with time after the mainshock. The healing rate was not constant but decreased logarithmically with time. In contrast, the apparent velocity changes are smaller than 0.5% registered at station E7 located at 175 away from the fault. The trend of healing rate decreasing with time after the mainshock is further shown in seismograms for 4 repeated aftershocks (Fig. 2a). The measured decreases in traveltime are ~30-50 ms in the first month, ~20-30 ms in the second month and less than ~15 ms in the third month after the mainshock, indicating again that post-seismic fault healing rate is not constant but decreased with time.

These measurements of traveltime changes with date show that shear velocities within the fault zone decreased by ~2.5% between R291 of 2002 and a week after the *M*6 Parkfield earthquake on September 28, 2004, most likely due to the co-seismic damage of rocks caused by crack opening during dynamic rupture of this *M*6 event. This change in velocity implies that the apparent crack density within the rupture zone was increased by 0.035 that caused 0.5% decrease in shear rigidity of fault-zone rock, according to the formula for seismic velocity in the cracked medium [*O'Connell and Budiansky*, 1974]. Then, *S* velocities increased by ~1.2% during ~3 months starting a week after the earthquake, indicating that the damaged rock has been healing and regaining the strength through rigidity recovery with time, most likely due to the closure of cracks that had opened during the mainshock. The healing rate was not constant with time but largest in the earlier stage of post-mainshock healing process. Our observations of fault zone damage and healing associated with the latest *M*6 Parkfield earthquake (Fig. 2b) are in general consistent with the model of velocity evolution owing to damage and healing for Lander and Hector Mine earthquakes [*Vidale and Li*, 2003]. However, the magnitude of damage and healing observed near Parkfield on the SAF is smaller than those on the Landers and Hector Mine rupture zones, probably related to the smaller magnitude mainshock, and smaller slip, and possibly differences in stress drop, pore-pressure, and rock type.

We then examined the data for variations in traveltime change along the fault strike and with depth. Fig. 3a exhibits the seismograms recorded at station within the fault zone for 2 repeated aftershocks in cluster 18 occurring at 4.6 km depth on October 11 and December 8, and other 2 repeated events in cluster 11 at 9.2 km depth on October 14 and December 5. Moving window waveform cross-correlations show larger decrease in wave traveltime for the pair of deeper aftershocks, although the time spans of repeated events in two pairs are nearly the same. This trend is shown for other 2 pairs of repeated aftershocks in cluster 12 at 3.7 km depth and in cluster 4 at 6.5 km, respectively. These observations suggest that the post-mainshock healing occurred on the ruptured fault to a depth of at least ~7 km. Fig. 3b shows relative decreases in traveltime for *S* and guided waves at 9 stations within 200-m-wide fault zone for 226 pairs of repeated aftershocks in 21 clusters measured by an automatic computer procedure for moving window cross-correlation. We used the data from repeated aftershocks with the first event occurring before October 26 (R300) and the second event occurred at least 20 days after the first event in the pair. The measured decreases in traveltime for pairs with longer time span between repeated aftershocks are normalized to the change in 20 days. This plot illustrates traveltime changes versus event depths, suggesting that the fault healing is most prominent at depths above 7 km. However, the measurements are scattered, probably due to the strong heterogeneity of the medium and the event location error, so that the depth-dependence of the damage-healing magnitude is not conclusive at this moment. We shall improve the measurements using the data from the SAFOD borehole recordings and the repeated events with updated locations in the Parkfield network catalogs through the proposed work.

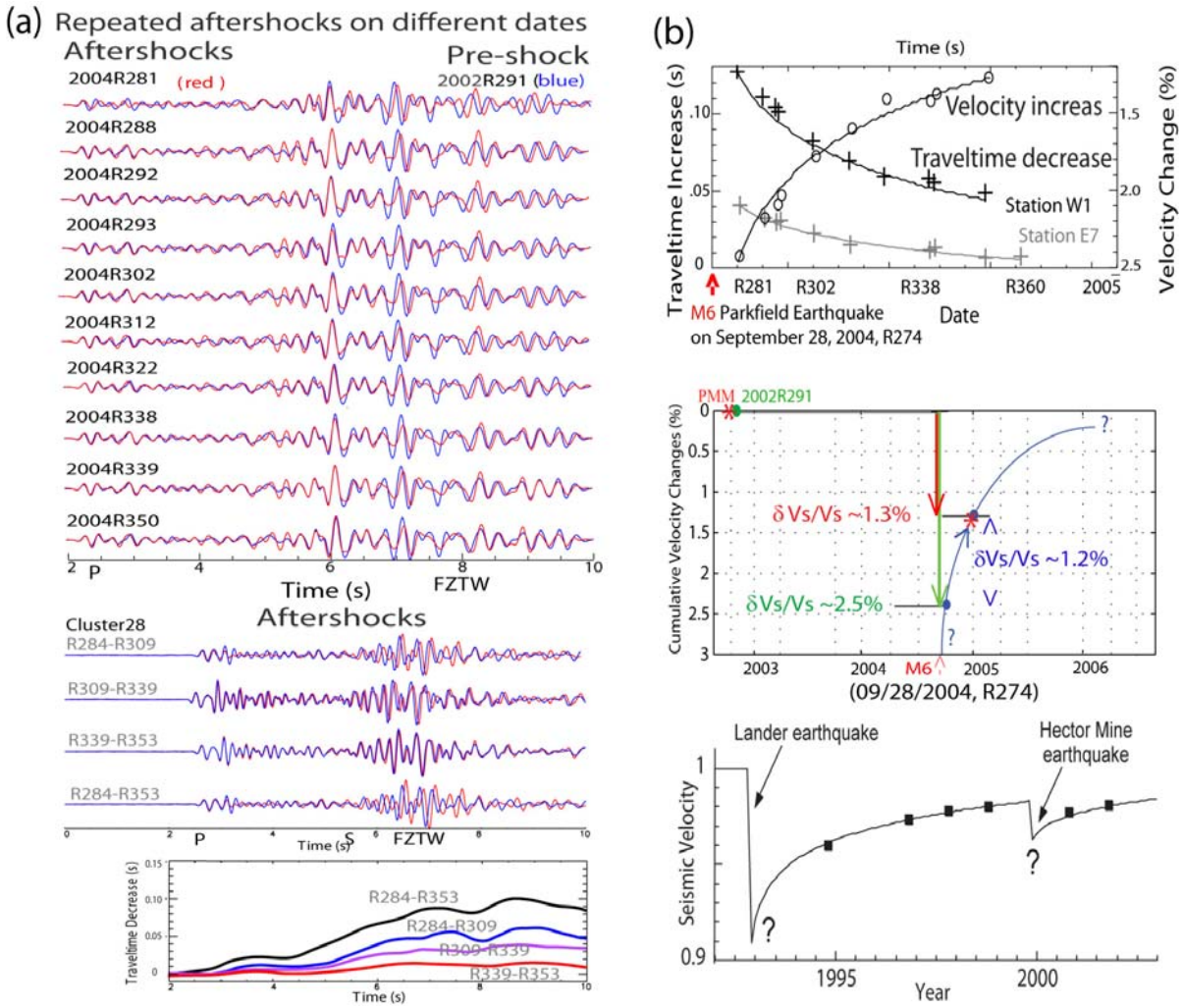

Figure 2 (a) Top: Vertical-component seismograms recorded at a station of the seismic array deployed within the fault zone for the microearthquake occurring on R291 in 2002 (blue line) and the 2004 Parkfield aftershocks (red lines) occurring at the same place, showing that waves traveled slower in 2004 with the largest time delay between the event in 2002 and the earliest aftershock in 2004 M6 Parkfield earthquake. The first *P*-arrivals are aligned. Mid: Vertical-component seismograms recorded at station W1 of array A for 4 repeated aftershocks in cluster 28 between Oct. 10 and Dec.17, 2004. Seismograms (<8 Hz filtered) are plotted for the earlier (red) and later events (blue) in each pair. Bottom: Moving-window cross-correlations of waveforms show that the travel-time advance in the pair of earlier repeated aftershocks is larger than that in the pair of later aftershocks. The time spans in the pairs are the same, indicating that the healing rate was larger in the earlier stage after the mainshock. First *P*-arrivals from repeated events are aligned at ~2.2 s. (b) Top: The maximum traveltime and shear velocity variations in percentage measured by moving-window cross-correlation of waveforms recorded at this station between the event in 2002 and 10 repeated events in 2004, showing the largest velocity reduction for the earliest repeated event and a increasing trend with dates after the mainshock.. Smaller changes were registered at station E7 farther away from the fault zone. The curve is the logarithmic fit to measurements of traveltime changes with a constant of velocity change 0.012 /day in logarithm. The velocity reduction is most likely due to co-seismic rock damage during the mainshock. The post-mainshock velocity increase suggests that the fault is recovering its rigidity with time. Mid: S-wave velocity changes within the rupture zone associated with the *M*6 Parkfield earth-quake on September 28, 2004. The *S* velocity decreased by ~1.3% in the time period between the two repeated shots on 16 October, 2002 and 28 December, 2004. Measurement for repeated microearthquakes occurring in 2002 and in a week after the 2004 *M*6 mainshock show ~2.5% decrease in *S* velocity, most likely due to the co-seismic rock damage during the mainshock. Measurements for repeated aftershocks show that the *S* velocity within the rupture zone increased by ~1.2% in the following 3 months starting, indicating fault healing with rigidity recovery of the damaged rocks. Bottom: The model of velocity changes as a function of time owing to combination of damage and healing at rupture zones of the 1992 *M*7.4 Landers and 1999 *M*7.1 Hector Mine earthquakes [*Vidale and Li*, 2003], shows healing as a logarithm of time.

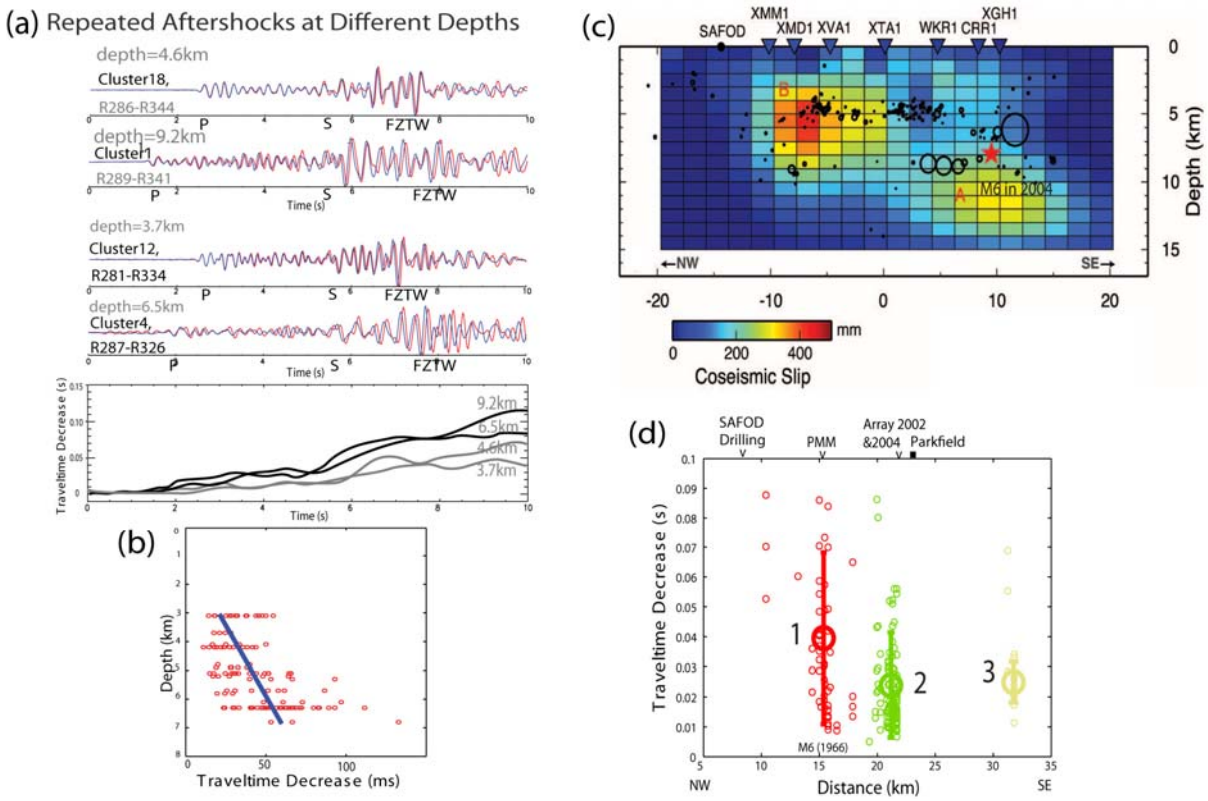

Figure 3 (a) Top: Vertical-component seismograms recorded at station W4 of array A for two repeated aftershocks in cluster 18 at 4.6 km depth and another two repeated events in cluster 11 at 9.2 km depth. Mid: Vertical-component seismograms at station W4 of array A for two repeated aftershocks in cluster 12 at 3.7 km depth and another two repeated events in cluster 4 at 6.5 km depth, showing again larger travel-time decreases for the pair of deeper aftershocks. Bottom: Moving-window waveform cross-correlations show that the travel-time decreases for the pair of deeper aftershocks are larger than those for the pair of shallower events, although time spans between the repeated events in two pairs are nearly the same. These observations suggest that the healing occurred on the SAF, likely across seismic depths to at least ~7 km, although with smaller healing magnitude within the deeper portion of the fault zone. (b) Travel-time decreases measured at nine stations W5–E3 located within the fault zone for 226 pairs of repeated aftershocks in 21 clusters, with the first event in each pair occurring before 26 October (R300) and the second event occurring at least 20 days later than the first event. The measured time decreases for each pair of repeated aftershocks have been normalized to the changes in 20 days. The straight line is the least squares fit to the data, showing that the accumulated travel-time advance increases as the event depth increases between depths of 3 km and 7 km. The results suggest that the fault experienced healing after the 2004 *M*6 Parkfield earthquake at seismogenic depths to ~7 km, although the magnitude of healing is smaller in the deeper portion of fault zone. (c) Results of inversion for co-seismic slip [Johanson et al., 2006]. The coseismic model plotted with the first day of aftershocks. Letters A & B refer to asperities. The greater damage and healing observed in our study (see Fig. 3d) are correlated to the larger slip. Alternatively, the observed post-mainshock healing might be affected by post-mainshock slips in creeping zone at shallow depths. (d) The data used in (b) are plotted versus distance of repeated aftershocks along the SAF strike. The mean values and standard deviations of the data for three groups of clusters labeled 1, 2, and 3 are marked by large circles and error bars. Group 1 is located close to the hypocenter of the 1966 *M*6 earthquake. The data have been normalized to a depth range of 4 km to remove the effect of different depths of pairs on measurements. Aftershocks in group 1 occurring on or close to the slip patch of the *M*6 earthquake in 1966 show larger travel-time decreases, although three groups of clusters are nearly at the same average depth.

Using the same data as in Fig. 3b, we plot the measured traveltime changes versus distance along the fault strike (Fig. 3d). The repeated aftershocks in group *1* located close to the hypocenter of the *M*6 earthquake in 1966 beneath Middle Mountain show relatively large changes in traveltime although the average depths of the

3 groups of clustered aftershocks used in this plot are nearly the same. *Langbein et al.* [2005] surveyed surface rupture and post mainshock surface slip after the 2004 September 28 *M*6 Parkfield earthquakes. They found the greatest dextral slip of 44 mm in the Middle Mountain area. The preliminary results from inverse of GPS and broadband waveform data also show the maximum slips of ~0.6 m at depths of 4-6 km beneath Middle Mountain [Johanson et al., 2006]. The greater damage and healing observed in our study (Fig. 3d) are correlated to the larger slip. We tentatively interpret that the greater damage was inflicted and thus greater healing is observed, in regions with larger co-seismic slips in the *M*6 mainshock. Alternatively, the observed post-mainshock healing might be affected by post-mainshock slips in creeping zone. We note that the measurements are scattered, but would be improved using the data with updated locations and the SAFOD borehole data.

Result from the data recorded at the SAFOD borehole seismographs

We examined the data for repeated aftershocks from the SAFOD borehole seismographs to confirm that the post-mainshock fault-zone heal could occur at seismogenic depths. For example, Figure 4a shows seismograms recorded at the mainhole and pilot-hole seismographs for a pair of aftershocks occurring at the similar locations within the fault zone at 5.7-km depth and 8 km southeast of the SAFOD site. Moving-window cross-correlations of mainhole seismograms for the two repeated events show ~15 ms advance of fault-zone trapped waves from the later aftershock on January 25 of 2005 than those from the aftershock on December 18 of 2004, occurring ~5 weeks before. However, there was no obvious time changes seen in pilot-hole seismograms for the same pair of repeated events. These observations show that the seismic velocities within the fault zone have been increased by ~0.3% during 10-15 weeks after the *M*6 Parkfield earthquake on September 28 of 2004, most likely due to fault healing with rigidity recovery of rocks that were damaged in the mainshock.

Figure 4b shows seismograms from the SAFOD boreholes for 3 repeated on0fault aftershocks occurring at 11 km depth and 14 km southeast of the SAFOD site on December 24 of 2004, and January 11 and 22 of 2005. Again, we observe that seismic waves from the later aftershocks traveled faster than those from the earlier aftershocks, showing the damaged fault-zone rocks in the *M*6 mainshock has been healing with time. We note that seismic waves traveled over longer distance show larger time advance (15 ms in Fig. 4b) than that (25 ms in Fig. 4a) over shorter distance, suggesting a roughly continuous damage zone on the Parkfield San Andreas fault along the fault strike and with depth in seismogenic crust. Based on the study in the current awarded project, we conclude that the low-velocity damage zone on the Parkfield San Andreas fault extends to the depth of at lease 6-7 km. A systematic analysis using all the recorded data will allow use to depict the variations in magnitude of co-seismic damage and post-mainshock healing on the SAF associated with the 2004 *M*6 Parkfield earthquake.

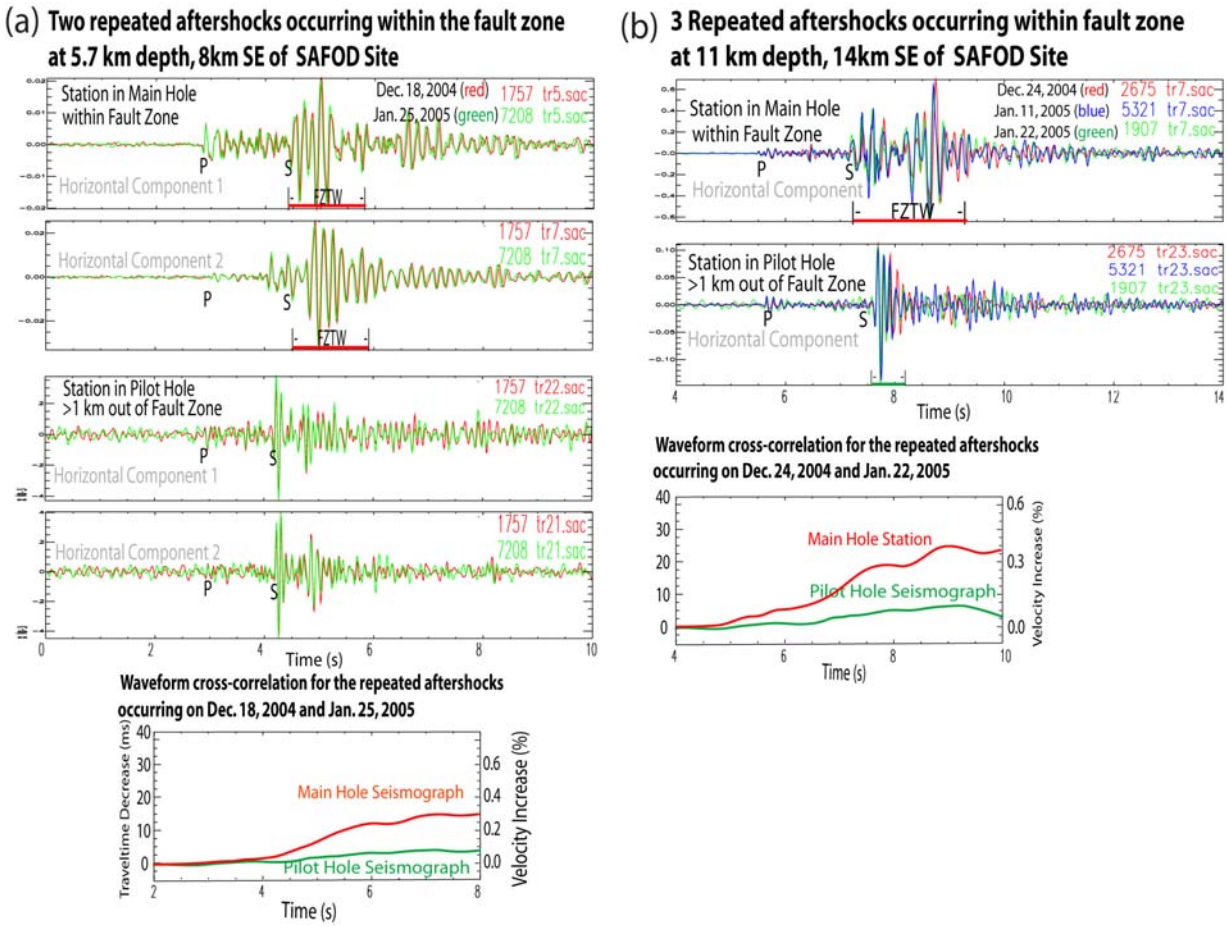

Figure 4 (a) Seismograms recorded at seismographs installed in the SAFOD mainhole and pilot hole in December of 2004 and later for repeated aftershocks occurring within the fault zone at depth of 5.7 km. Waveform cross-correlations for the repeated events show ~0.3% velocity increase within the fault zone in 5 weeks starting 10 weeks after the *M*6 mainshock, indicating that the fault zone rocks damaged in the mainshock have being healing with time. The heal process was seen within the fault zone at depths below 3 km, but not seen far away from the fault zone. (b) Borehole seismograms for two repeated aftershocks occurring within the fault zone at depths of 11 km, showing that waves from the later event traveled faster than the earlier event. Waveform cross-correlations for the repeated events show ~0.35% velocity increase within the fault zone in 5 weeks, starting 80 days after the *M*6 mainshock, but no changes seen at 1.8 km away from the fault zone, suggesting that the deep portion of the fault zone experienced damage and healing associated with the 2004 *M*6 Parkfield earthquake.